Multi-responsive thiosemicarbazone-based probe for detection and discrimination of group 12 metal ions and its application in logic gate

Soma Sarkar, Tapashree Mondal, Swapnadip roy, Raj Narayan Saha, Ashish K Ghosh and Sujit S. Panja*

Table of Contents

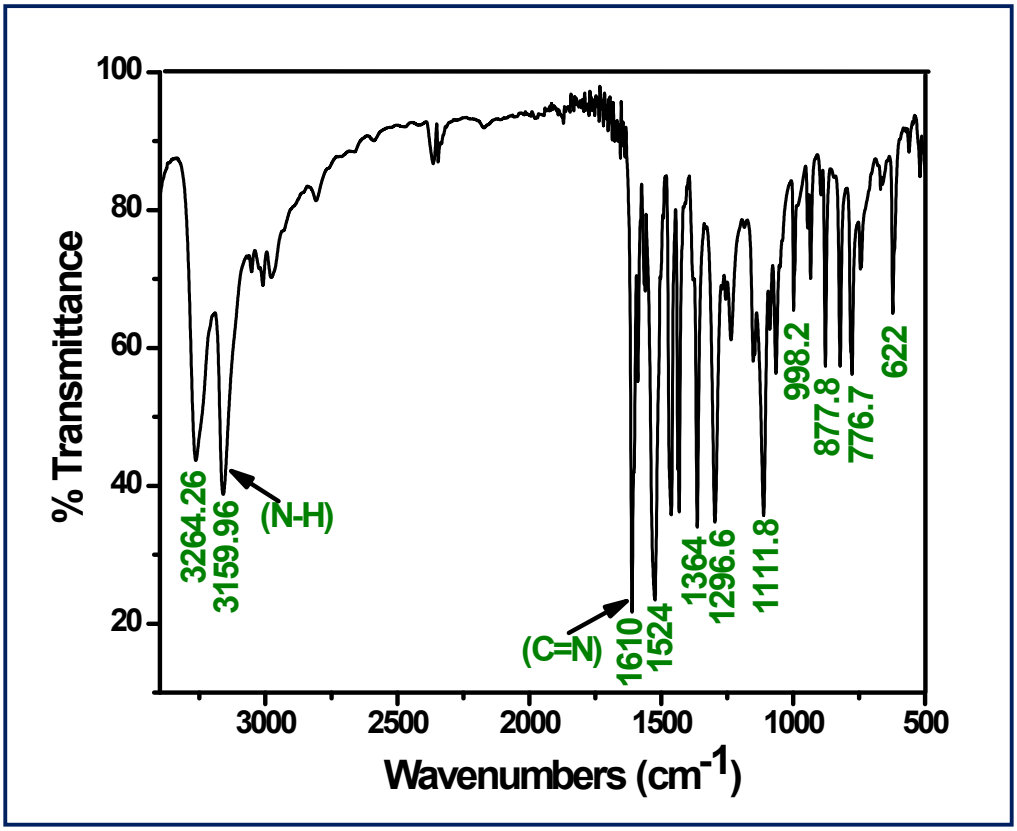

Fig. S1. FTIR spectrum of **L.**

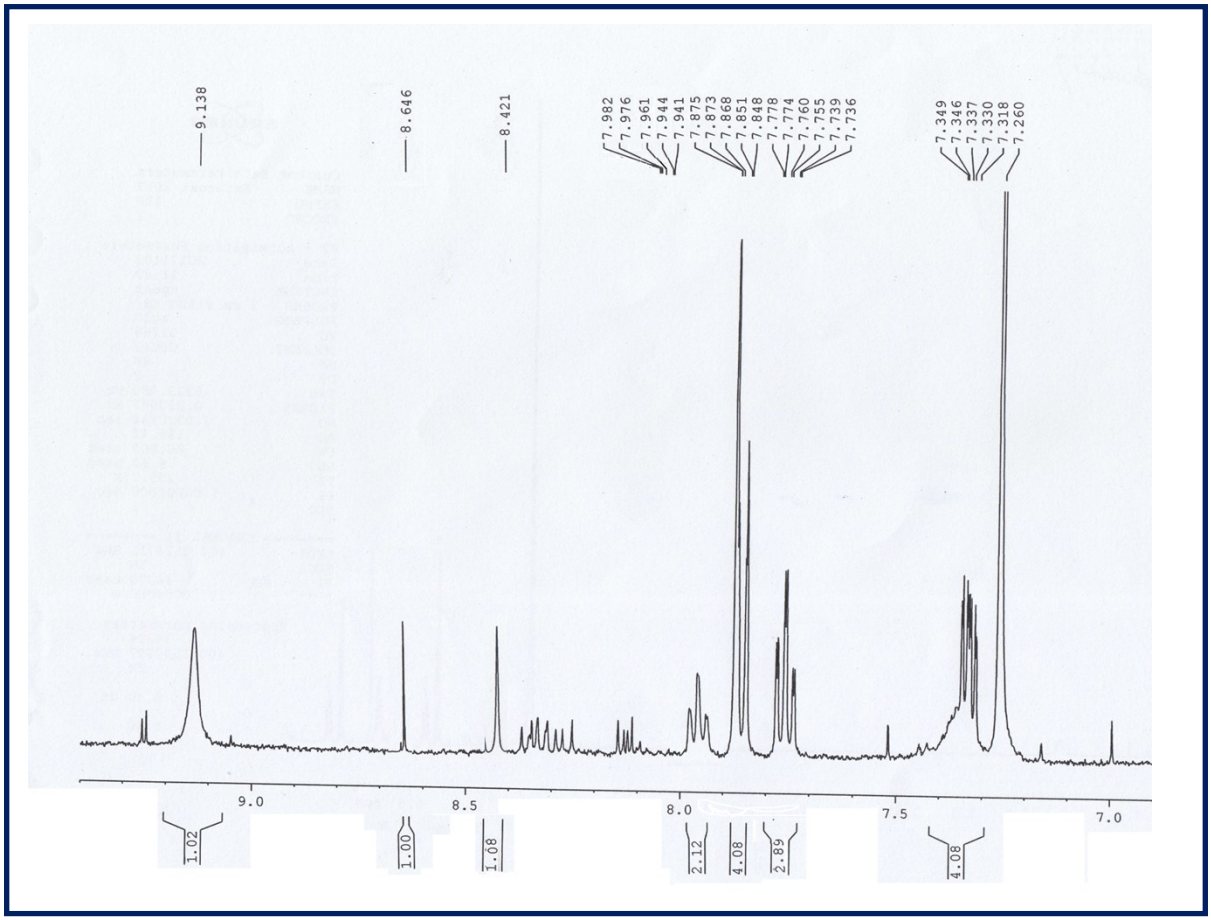

Fig. S2. ^{1}H NMR spectrum of **L.**

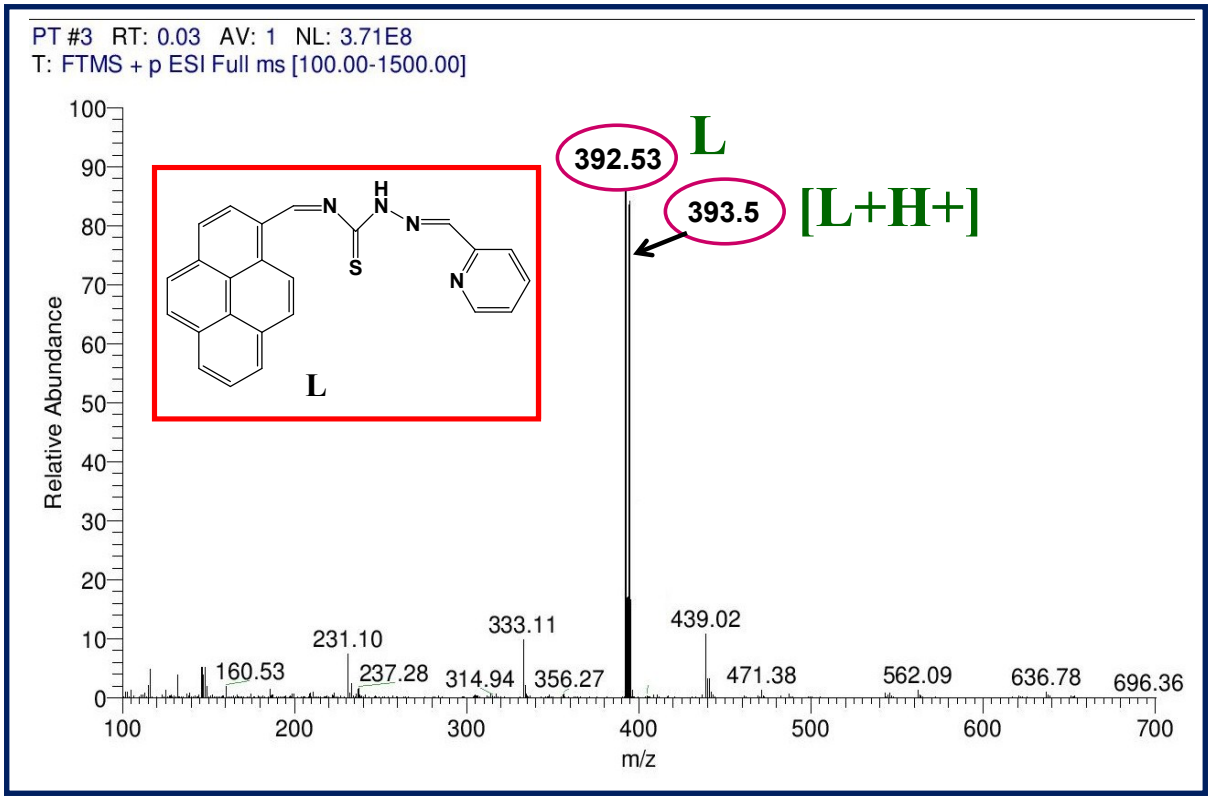

Fig. S3. Mass spectrum of **L.**

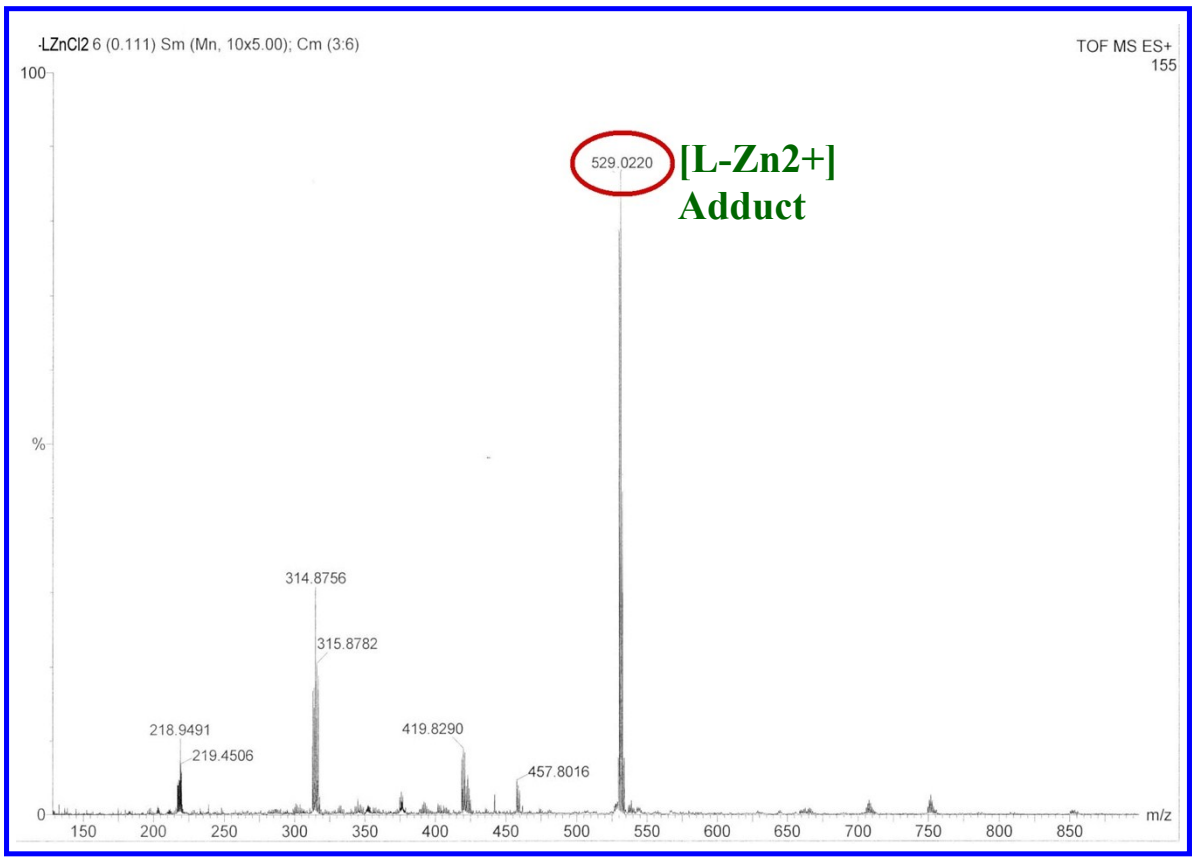

Fig. S4. Mass spectrum of [**L**-Zn^{2+}] adduct.

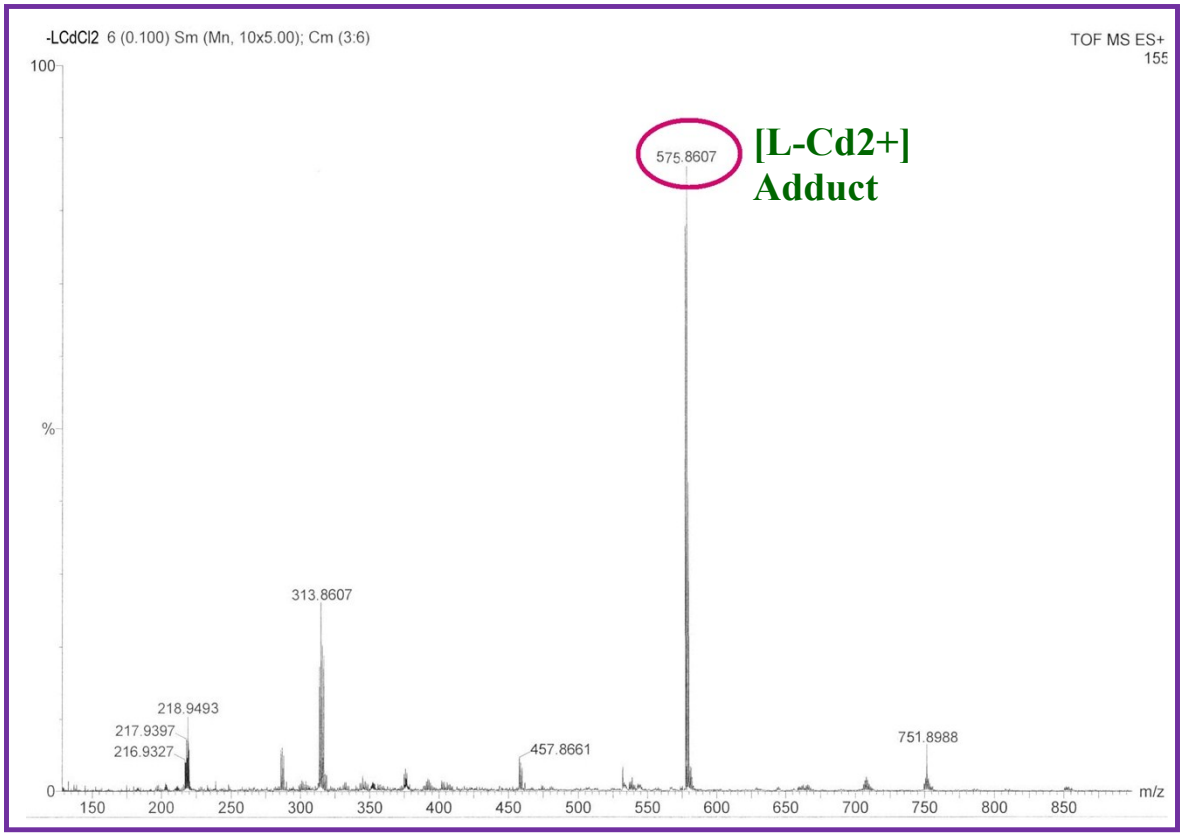

Fig. S5. Mass spectrum of [**L**-Cd^{2+}] adduct.

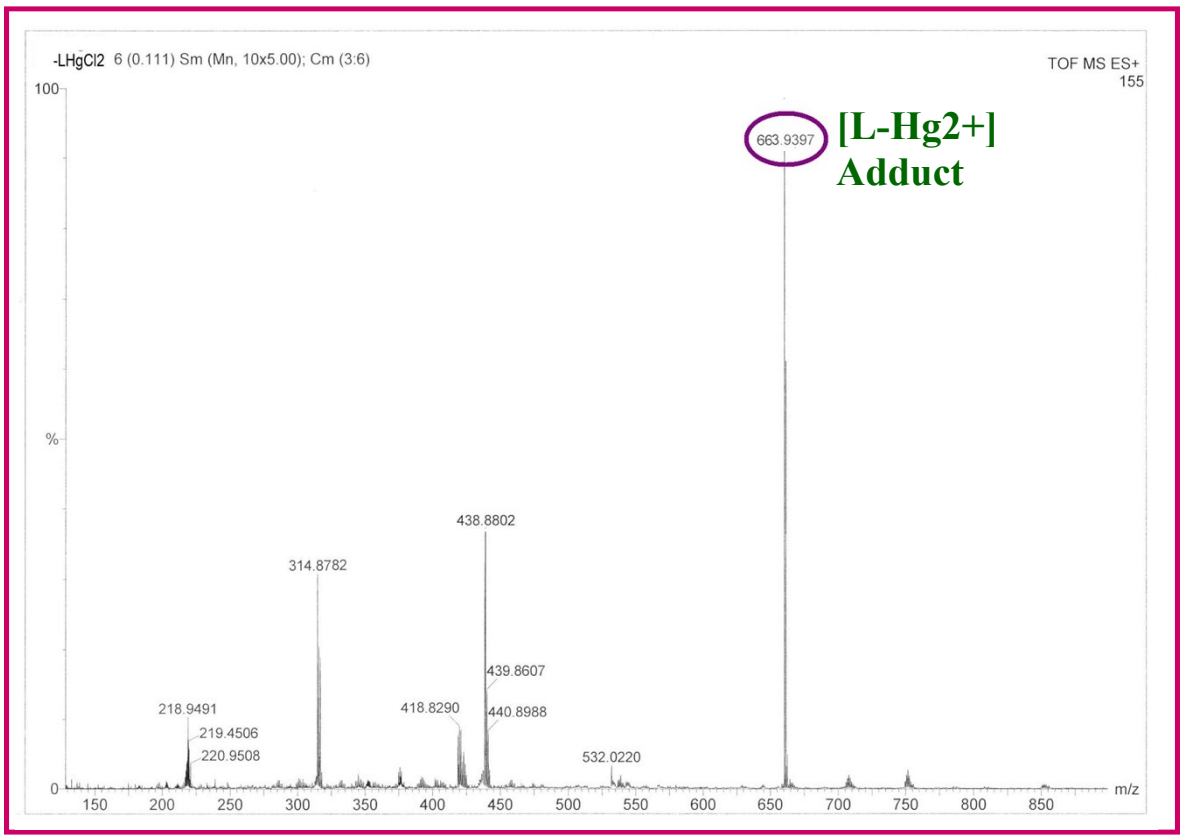

Fig. S6. Mass spectrum of [**L**-Hg^{2+}] adduct.

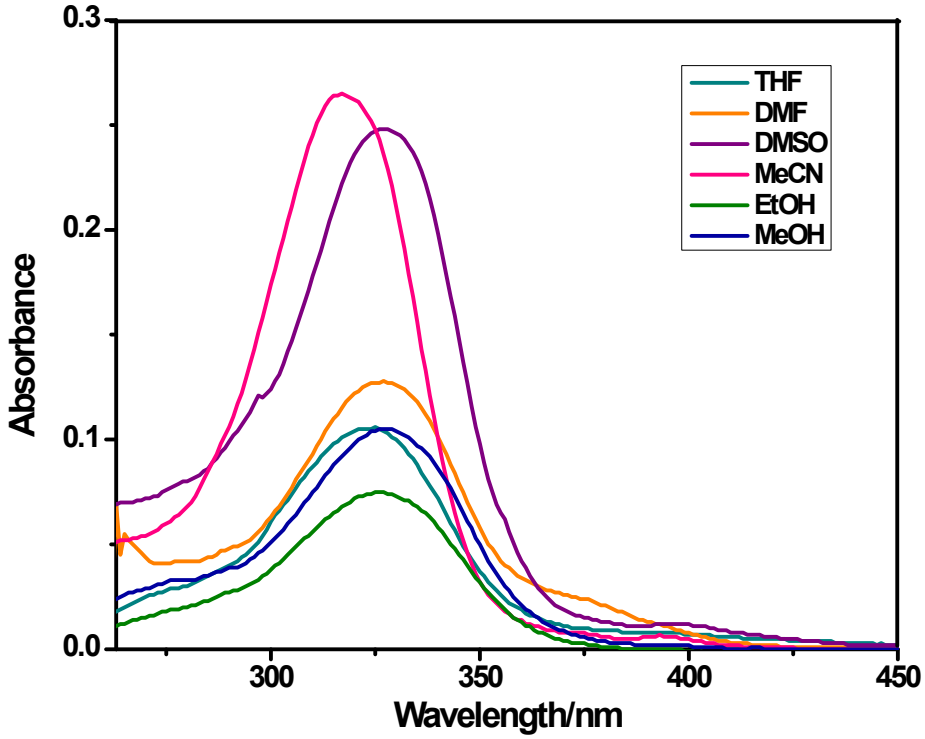

Fig. S7. UV-Vis absorption spectra of **L** (5 μM) in different solvents.

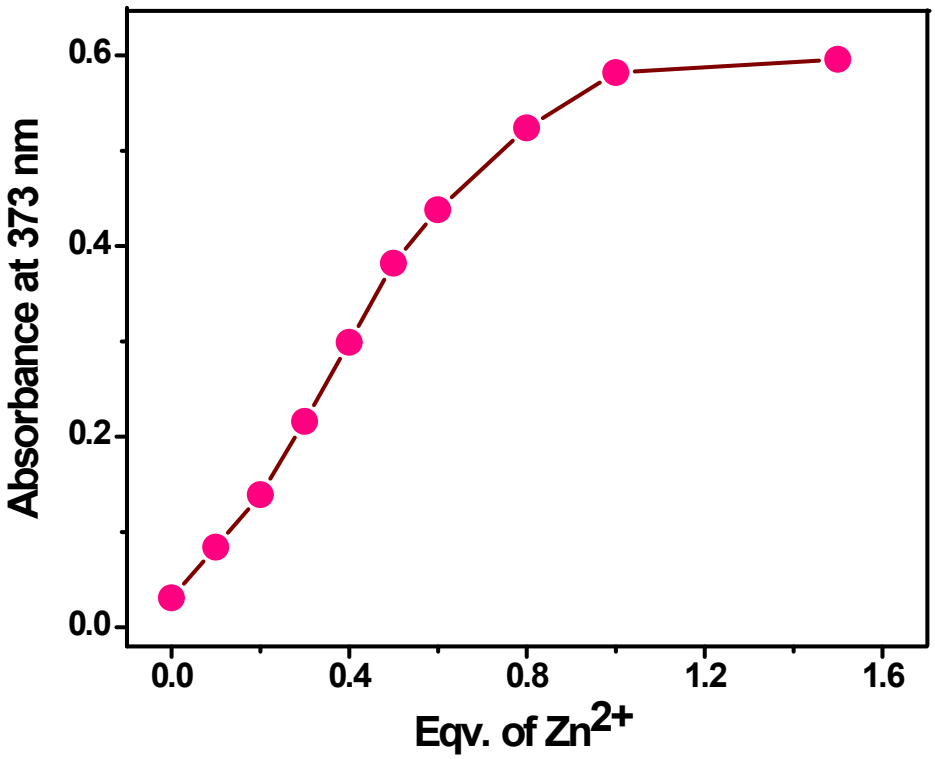

Fig. S8. Changes of absorbance at λ_{max} = 373 nm as a function of equivalents of Zn^{2+}.

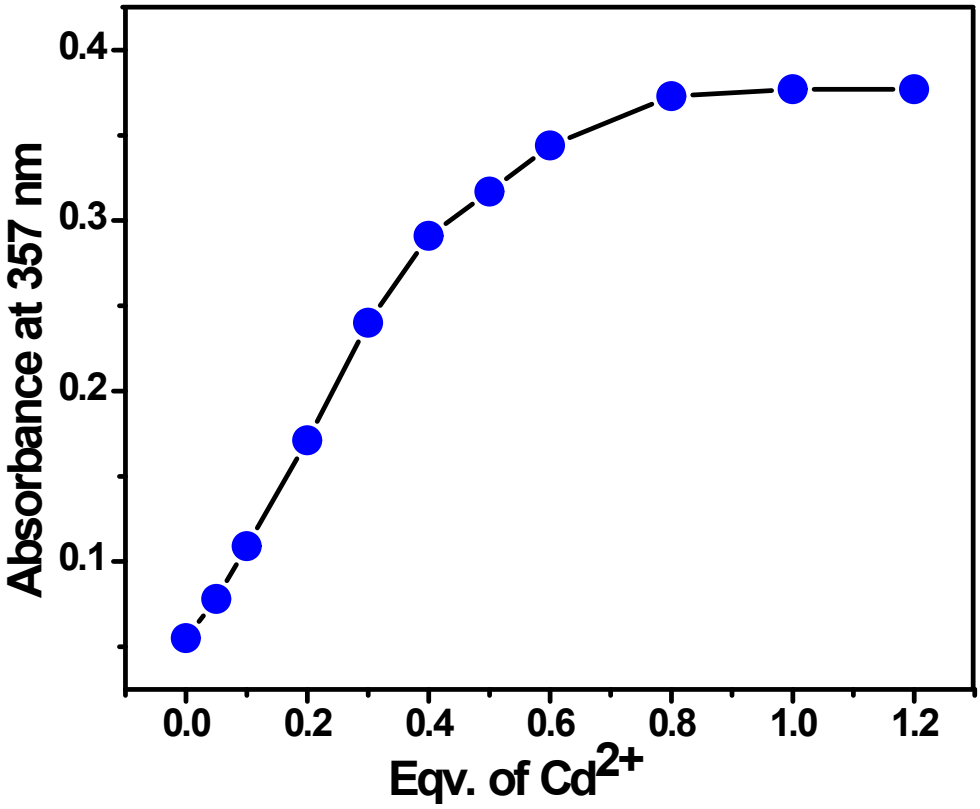

Fig. S9. Changes of absorbance at λ_{max} = 357 nm as a function of equivalents of Cd^{2+}.

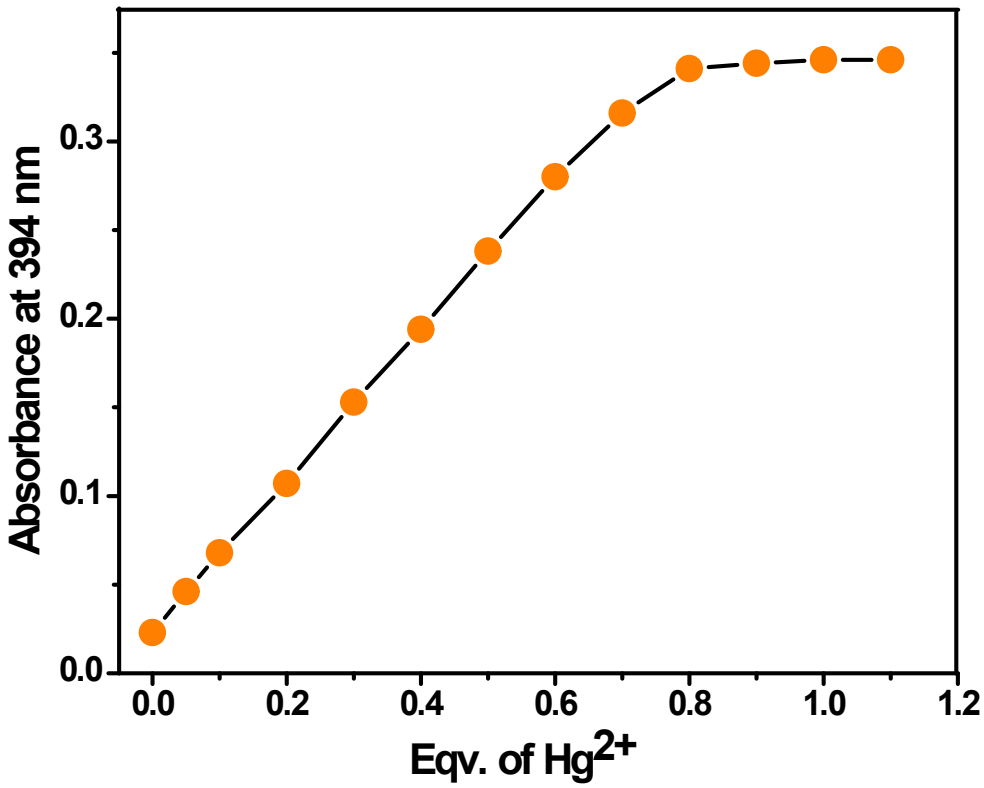

Fig. S10. Changes of absorbance at λ_{max} = 394 nm as a function of equivalents of Hg^{2+}.

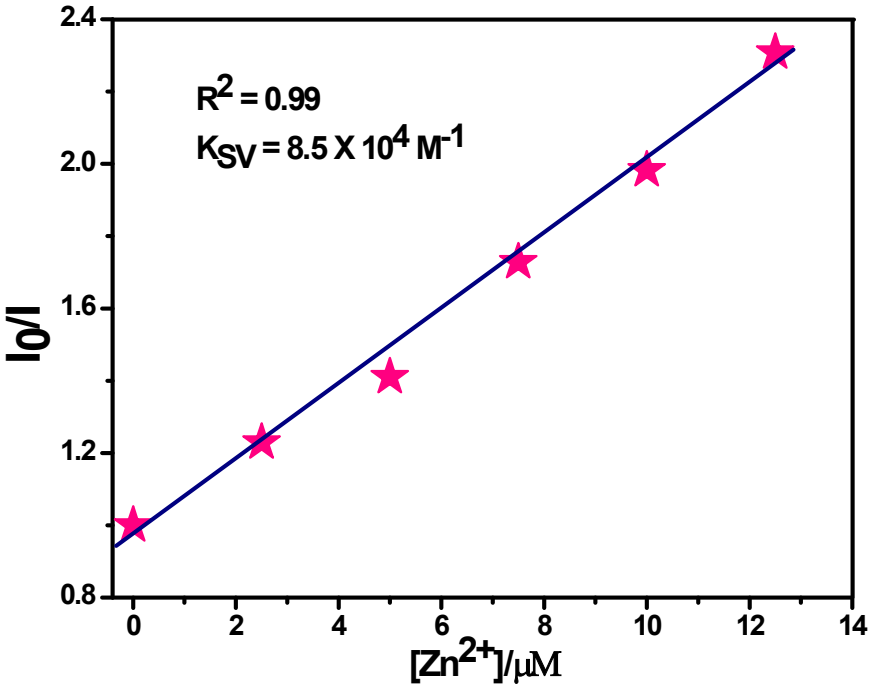

Fig. S11. Stern–Volmer plot for **L** as a function of Zn^{2+} concentration.

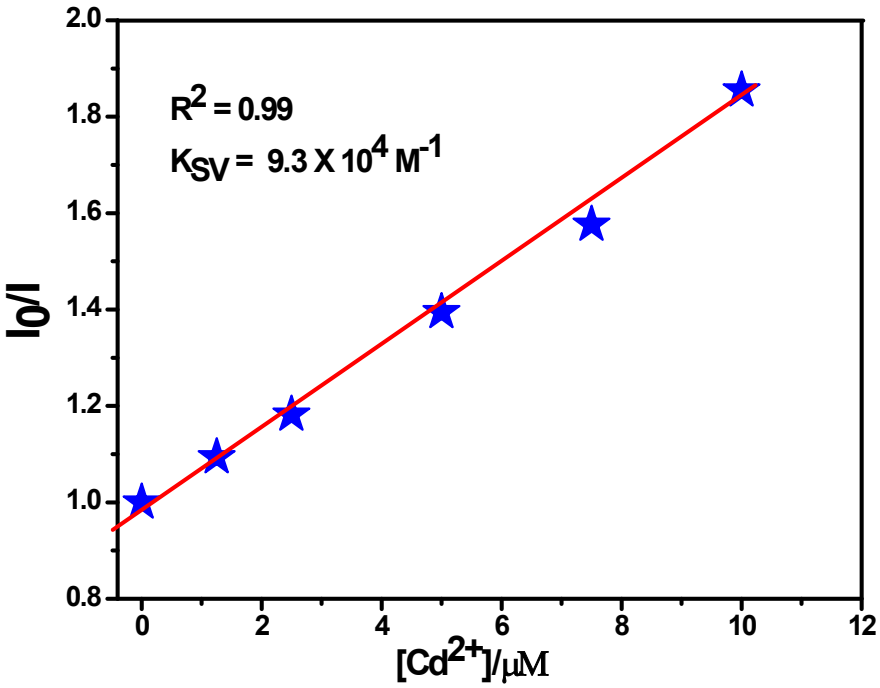

Fig. S12. Stern–Volmer plot for **L** as a function of Cd^{2+} concentration.

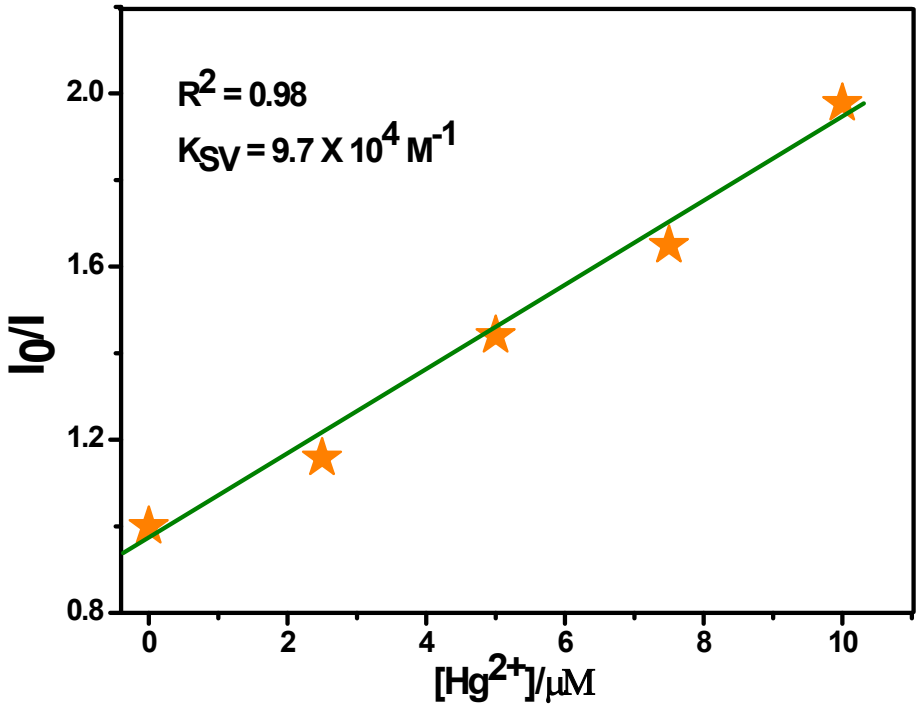

Fig. S13. Stern–Volmer plot for **L** as a function of Hg^{2+} concentration.

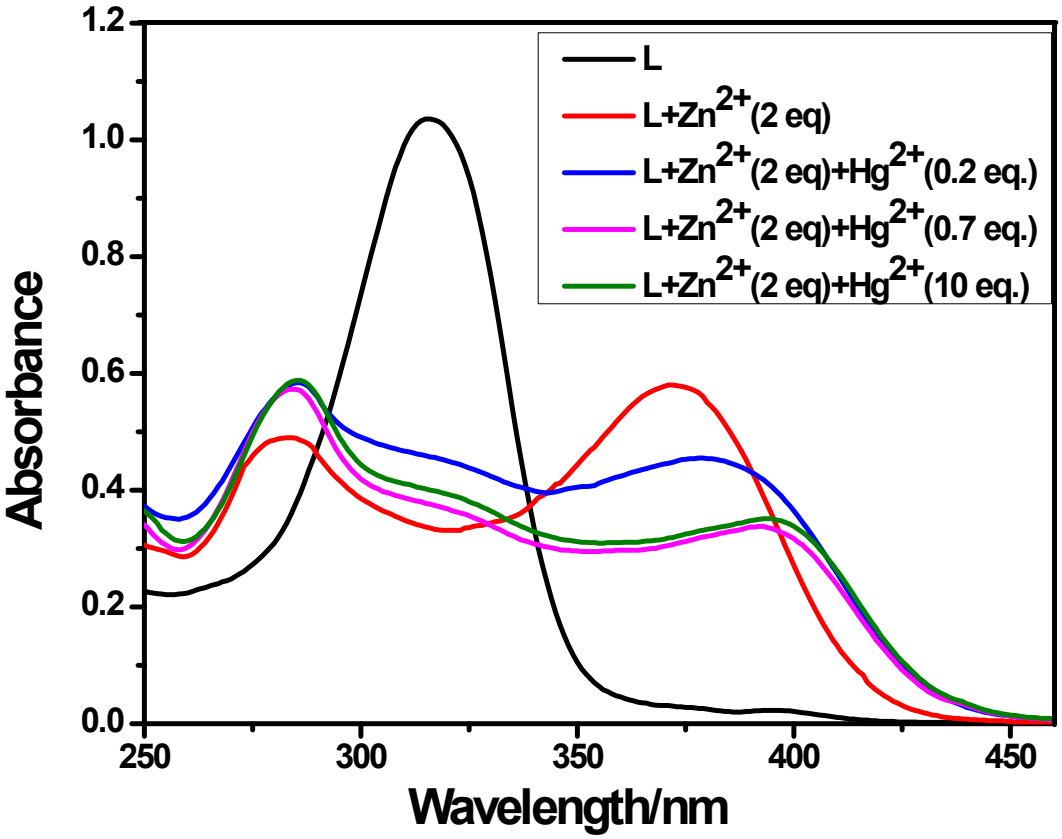

Fig. S14. Changes in the absorption spectra of [**L**-Zn^{2+}] adduct upon addition of Hg^{2+} in Tris buffered MeCN/H_2O (1:1, v/v, pH = 7) solution.

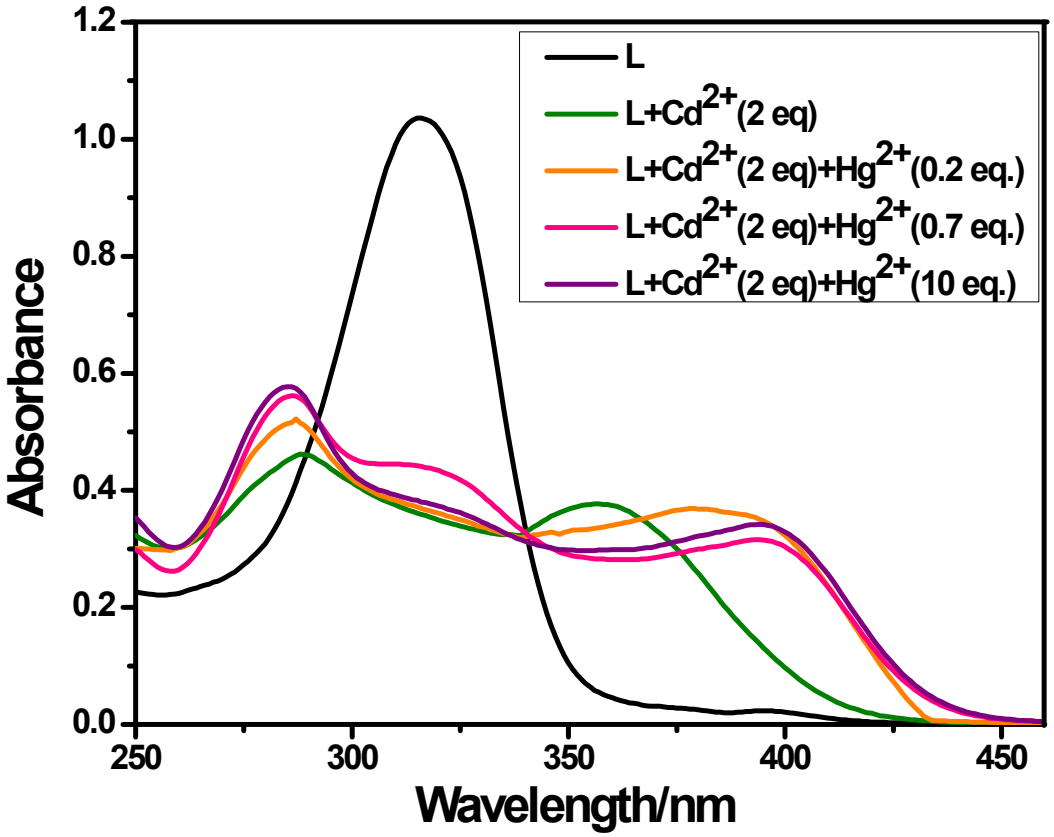

Fig. S15. Changes in the absorption spectra of [**L**-Cd^{2+}] adduct upon addition of Hg^{2+} in Tris buffered MeCN/H_2O (1:1, v/v, pH = 7) solution.

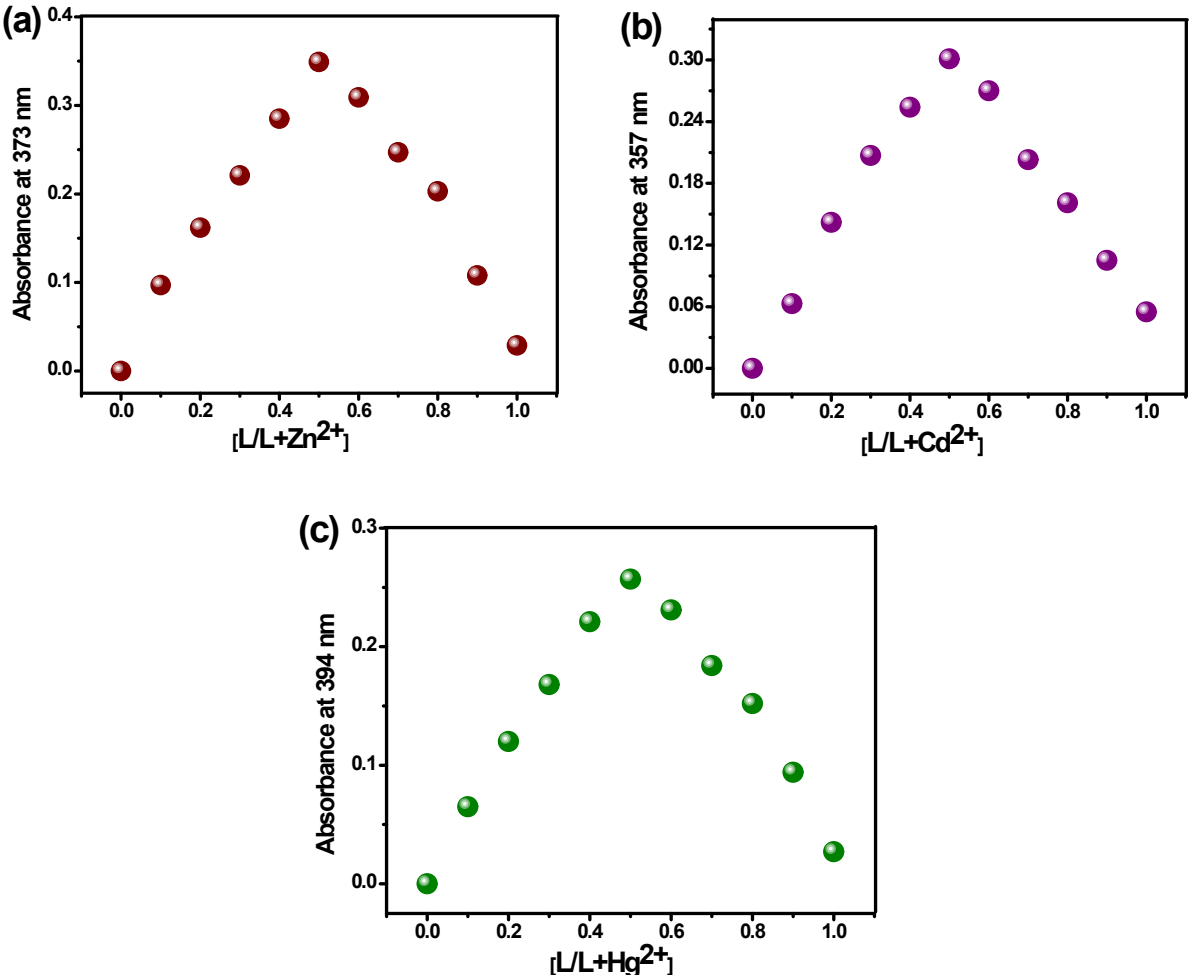

Fig. S16. Jobs plot for determining the stoichiometry of **L** and (a) Zn^{2+} adduct at λ_{max} = 373 nm, (b) Cd^{2+} adduct at λ_{max} = 357 nm, (c) Hg^{2+} adduct at λ_{max} = 394 nm in Tris-HCl buffered (10 mM, pH =7) MeCN/H_2O (v/v = 1:1). Total concentration = 25 μM.

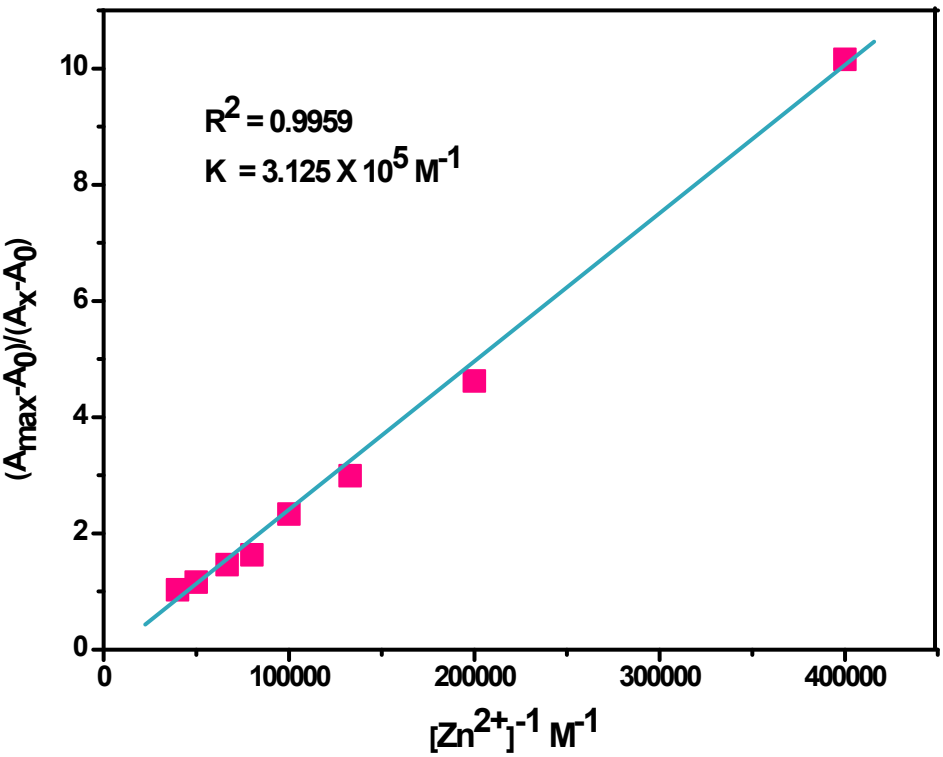

Fig. S17. Benesi-Hildebrand plot for determination of the binding constant of **L** with Zn^{2+} using the absorbance technique.

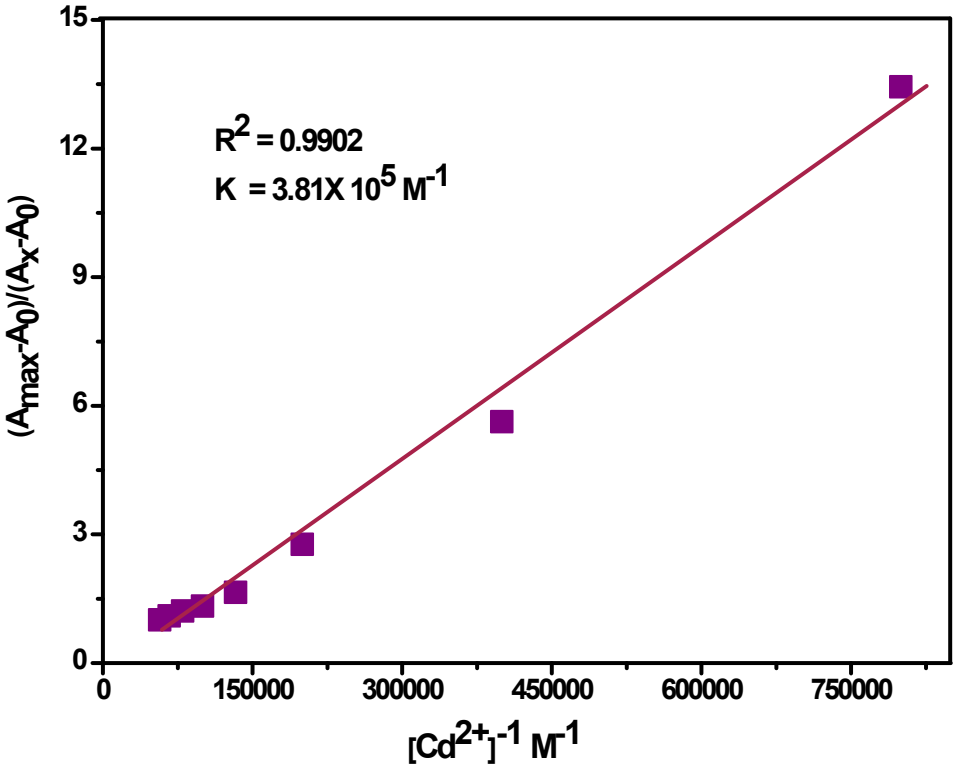

Fig. S18. Benesi-Hildebrand plot for determination of the binding constant of **L** with Cd^{2+} using the absorbance technique.

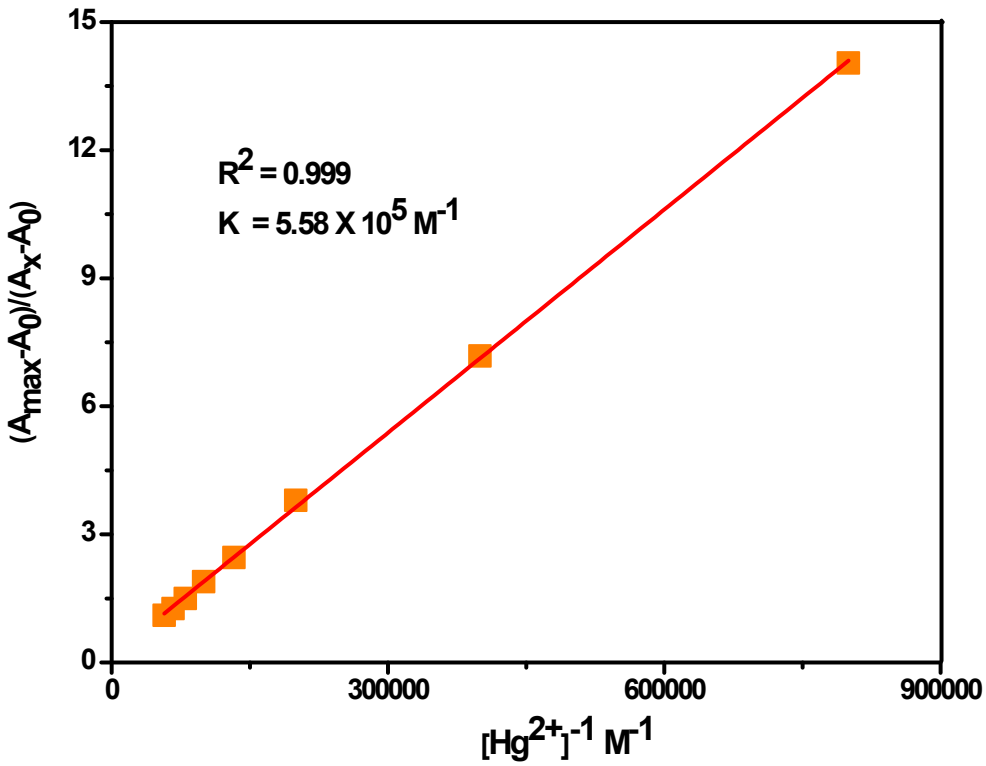

Fig. S19. Benesi-Hildebrand plot for determination of the binding constant of **L** with Hg^{2+} using the absorbance technique.

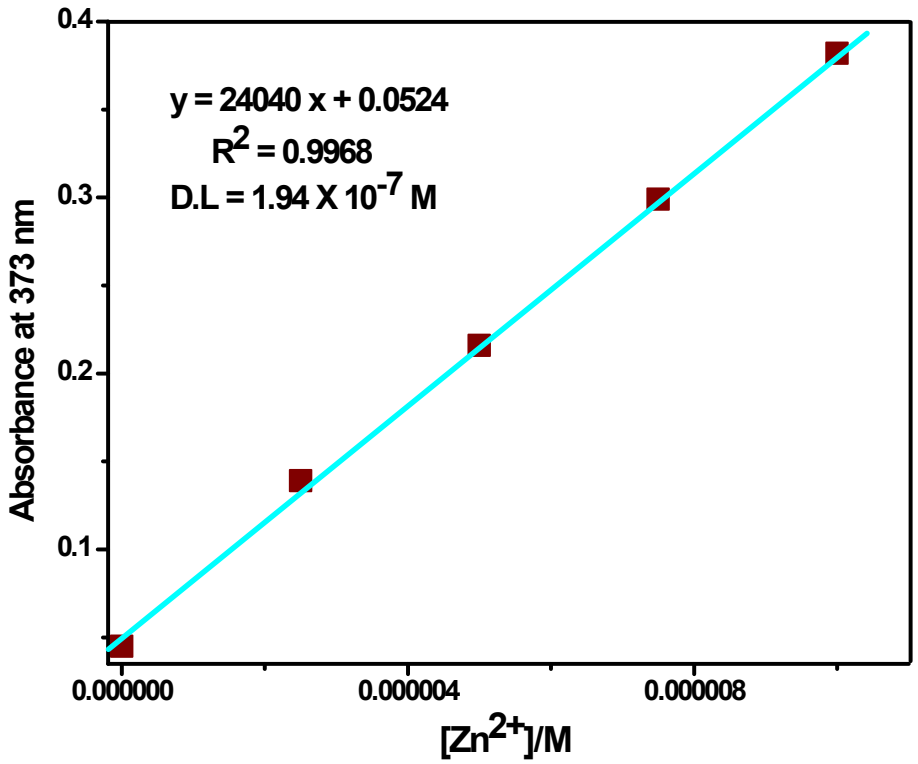

Fig. S20. The detection limit of **L** for Zn^{2+} by absorbance technique.

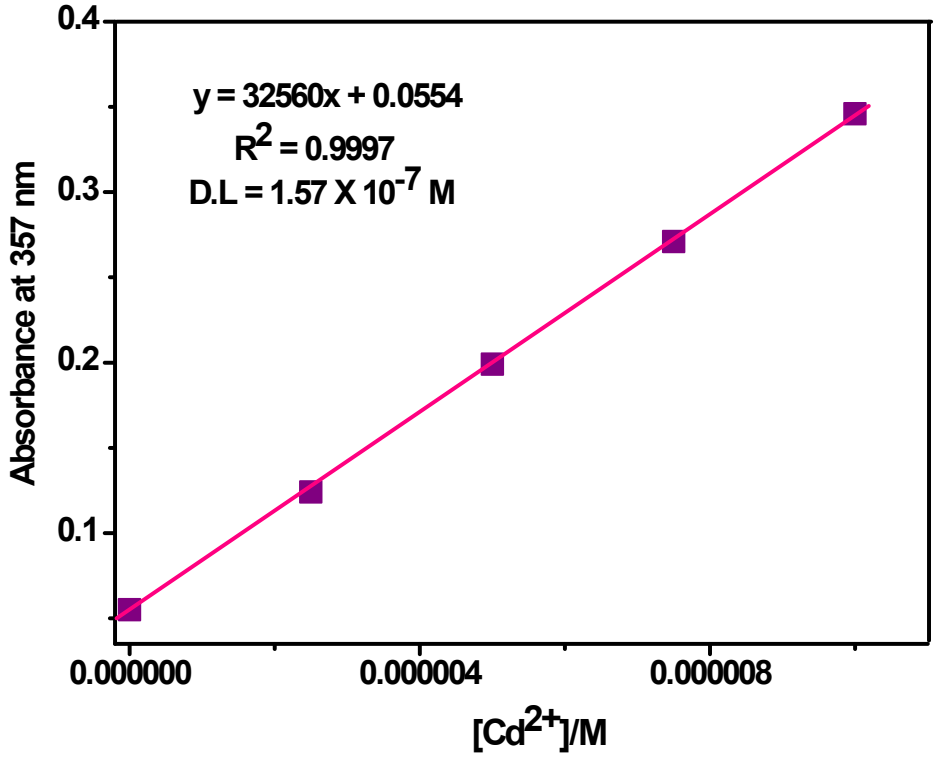

Fig. S21. The detection limit of **L** for Cd^{2+} by absorbance technique.

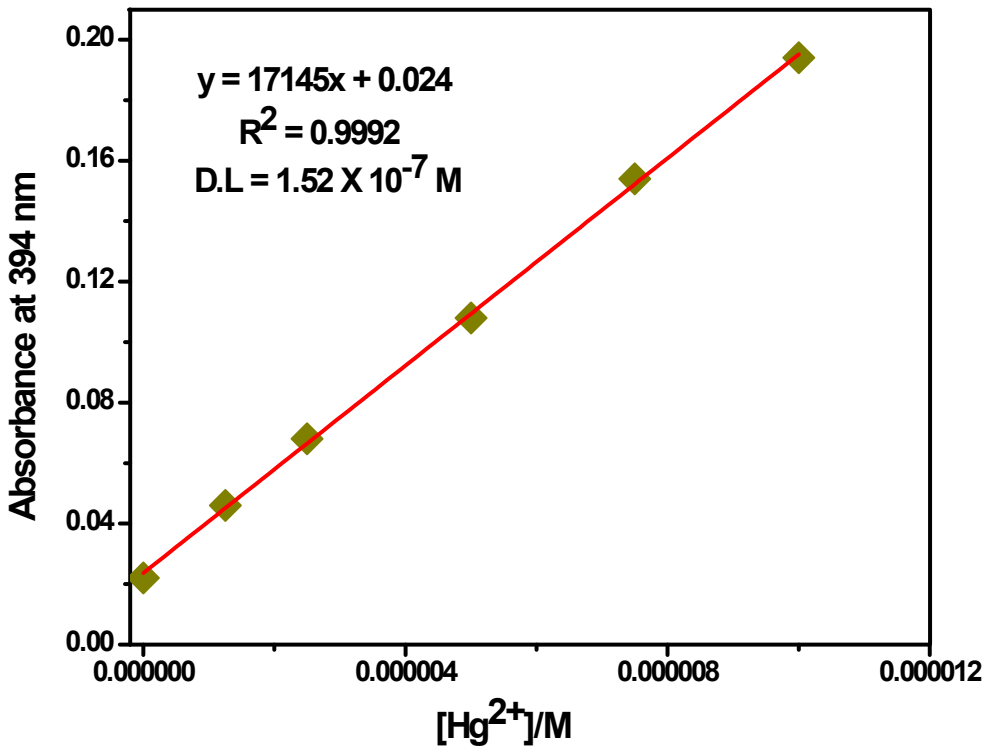

Fig. S22. The detection limit of **L** for Hg^{2+} by absorbance technique.

Absorbance at λmax = 316 nm

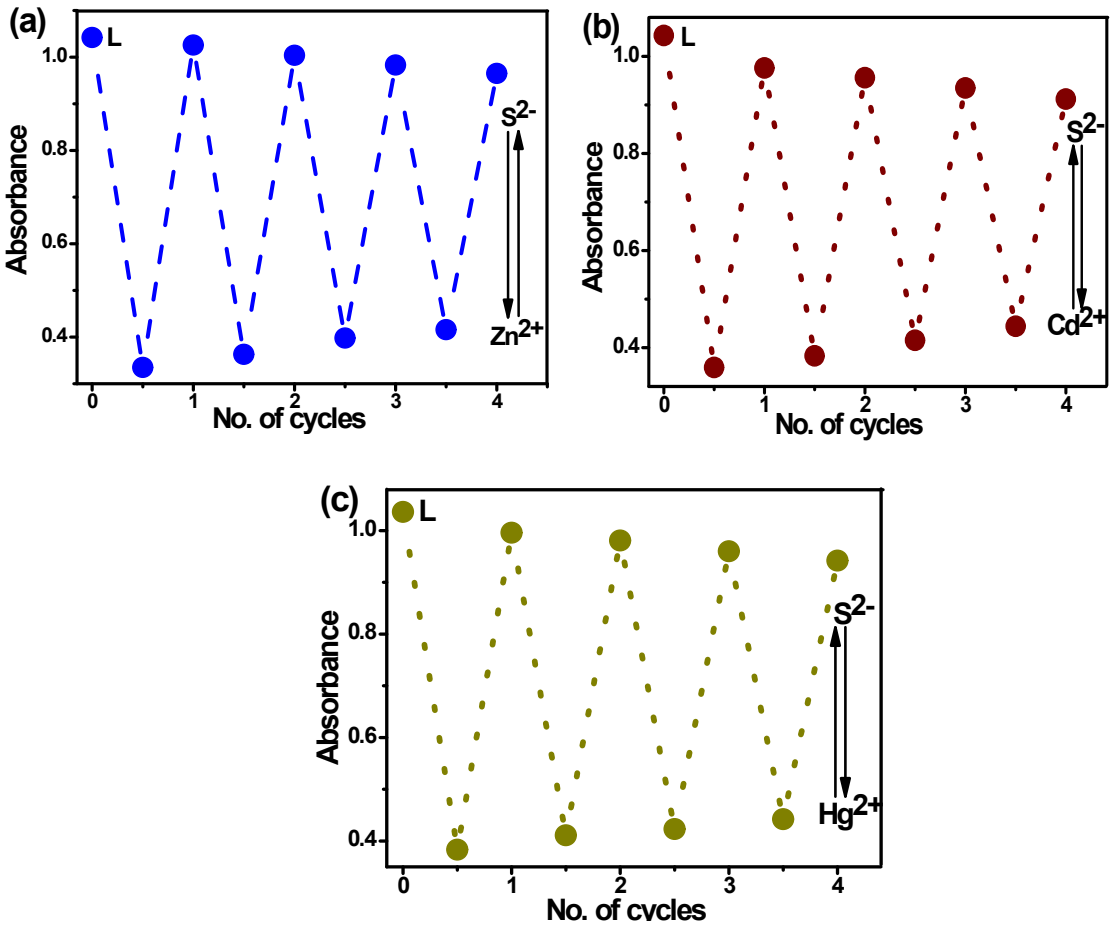

Fig. S23. Representative bar chart diagram for showing the change of absorbance at λ_{max} = 316 nm by adding various anions (100 μM) to solution of [**L**-Zn^{2+}] (blue bars), [**L**-Cd^{2+}] (red bars) and [**L**-Hg^{2+}] (green bars) complexes. 1 = Cl^-, 2 = F^-, 3 = SO_4^{2-}, 4 = OAc^-, 5 = NO_3^-, 6 = Br^-, 7 = S^{2-}. Sensing-recovery cycles for **L** (25 μM) at λ_{max} = 316 nm upon addition of **(a)** Zn^{2+} (25 μM), **(b)** Cd^{2+} (25 μM) and **(c)** Hg^{2+} (25 μM) and subsequent regeneration by S^{2-} (50 μM). Dotted lines serve guide to eyes.

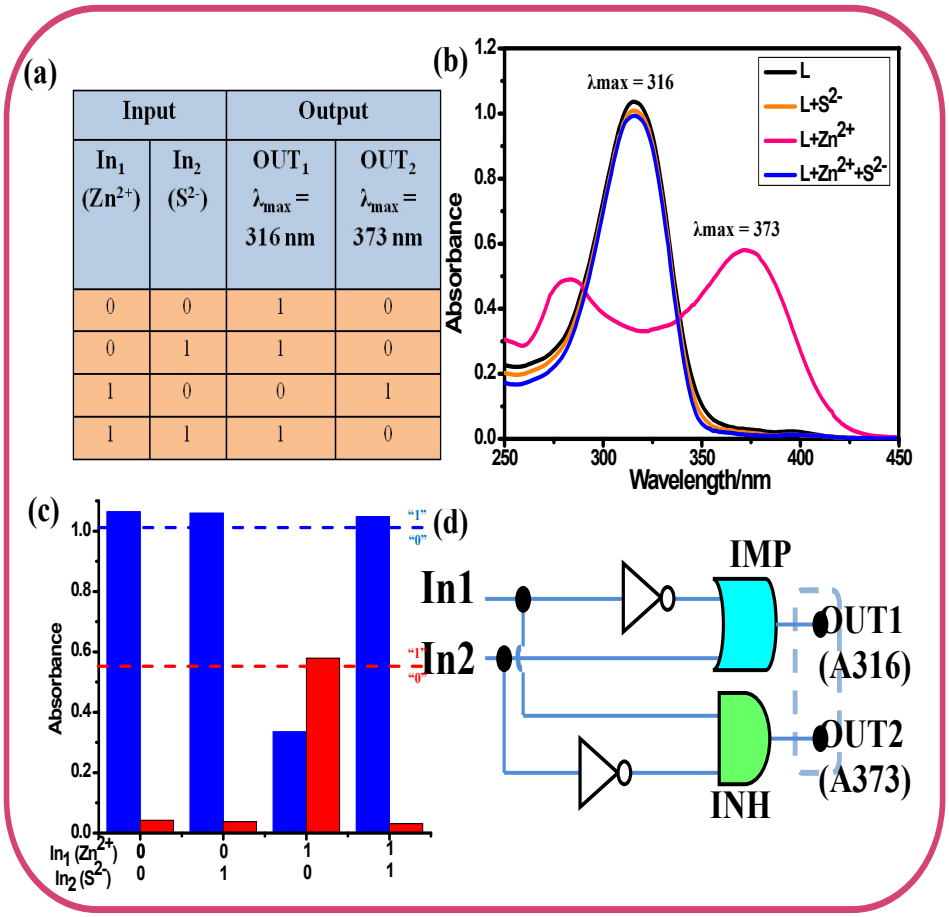

Fig. S24. (a) Truth table of the logic gate, (b) Output signals of the logic gate in presence of different inputs, (c) corresponding bar diagram of absorbance outputs of **L** at λ_{max} = 316 nm (OUT_1, blue bars) and λ_{max} = 373 nm (OUT_2, red bars) in presence of two chemical inputs: In_1 (Zn^{2+}) and In_2 (S^{2-}) and (d) the corresponding logic circuit.

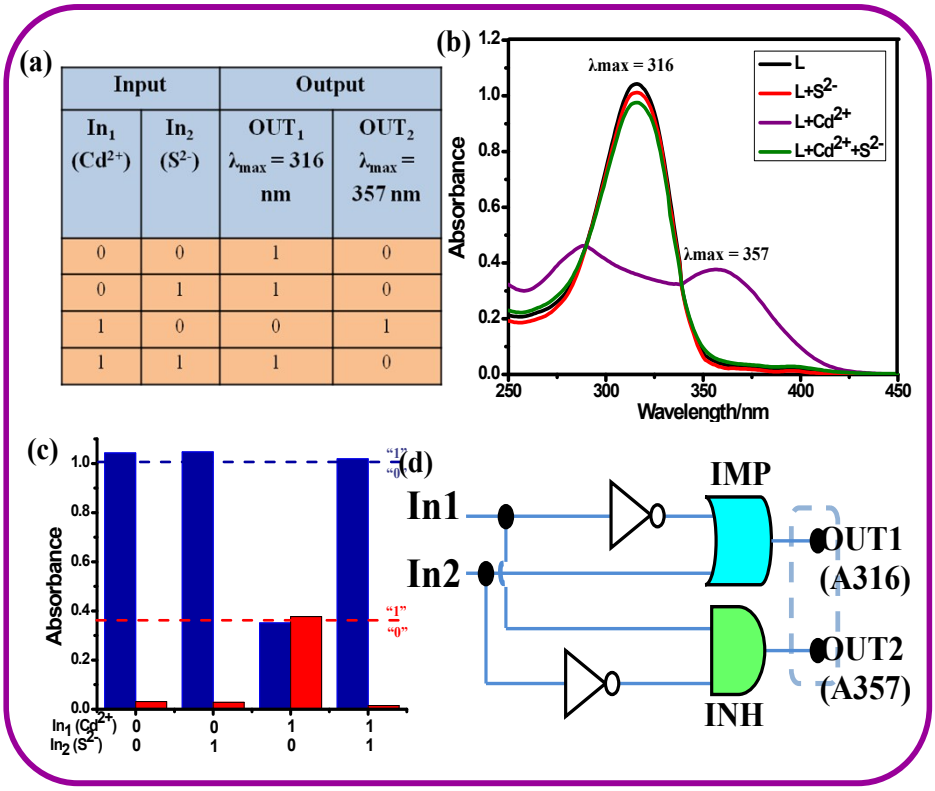

Fig. S25. (a) Truth table of the logic gate, (b) Output signals of the logic gate in presence of different inputs, (c) corresponding bar diagram of absorbance outputs of **L** at λ_{max} = 316 nm (OUT_1, blue bars) and λ_{max} = 357 nm (OUT_2, red bars) in presence of two chemical inputs: In_1 (Cd^{2+}) and In_2 (S^{2-}) and (d) the corresponding logic circuit.

Table S1. Data from theoretical TDDFT studies of **L**

Compound	Electronic Transitions	Energy (eV)	Wavelength (nm)	f^b	Transitions involved
L	S_0-S_1	0.6569 eV	387.31 nm	0.0361	HOMO→LUMO HOMO→LUMO+1
	S_0-S_2	1.3969 eV	317.58 nm	0.0126	HOMO→LUMO+2 HOMO→LUMO+3
	S_0-S_3	1.6689 eV	262.90 nm	0.0020	HOMO-2→LUMO HOMO-1→LUMO HOMO→LUMO HOMO→LUMO+1 HOMO-1→LUMO

Table S2. Data from theoretical TDDFT studies of complexes

Compound	Electronic Transitions	Energy (eV)	Wavelength (nm)	f[b]	Transitions involved
(**L**-Zn^{2+}) complex	S_0-S_1	0.7156 eV	422.53 nm	0.0676	HOMO→LUMO HOMO→LUMO+1
	S_0-S_2	1.2632 eV	381.48 nm	0.0032	HOMO-1→LUMO
	S_0-S_3	1.2949 eV	269.49 nm	0.0011	HOMO-1→LUMO
(**L**-Cd^{2+}) complex	S_0-S_1	0.3450 eV	406.09 nm	0.0050	HOMO→LUMO HOMO→LUMO+1
	S_0-S_2	0.4097 eV	369.75 nm	0.0577	HOMO→LUMO HOMO→LUMO+1
	S_0-S_3	1.6215 eV	264.63 nm	0.0398	HOMO-1→LUMO HOMO→LUMO+2 HOMO-1→LUMO HOMO-1→LUMO+1 HOMO-1→LUMO+2
(**L**-Hg^{2+}) complex	S_0-S_1	0.3673 eV	475.81 nm	0.0472	HOMO→LUMO HOMO→LUMO+2
	S_0-S_2	1.4707 eV	413.00 nm	0.0031	HOMO→LUMO+1 HOMO-1→LUMO HOMO-1→LUMO+2
	S_0-S_3	1.5599 eV	292.80 nm	0.0225	HOMO→LUMO+1 HOMO→LUMO+2